

1

2 **A large-scale systematic survey of SARS-CoV-2 antibodies**

3 **reveals recurring molecular features**

4

5 Yiquan Wang^{1,*}, Meng Yuan^{2,*}, Jian Peng³, Ian A. Wilson^{2,4}, Nicholas C. Wu^{1,5,6,7,§}

6

7

8 ¹Department of Biochemistry, University of Illinois at Urbana-Champaign, Urbana, IL 61801,
9 USA

10 ²Department of Integrative Structural and Computational Biology, The Scripps Research
11 Institute, La Jolla, CA 92037, USA

12 ³Department of Computer Science, University of Illinois at Urbana-Champaign, Urbana, IL
13 61801, USA

14 ⁴The Skaggs Institute for Chemical Biology, The Scripps Research Institute, La Jolla, CA
15 92037, USA

16 ⁵Center for Biophysics and Quantitative Biology, University of Illinois at Urbana-Champaign,
17 Urbana, IL 61801, USA

18 ⁶Carl R. Woese Institute for Genomic Biology, University of Illinois at Urbana-Champaign,
19 Urbana, IL 61801, USA

20 ⁷Carle Illinois College of Medicine, University of Illinois at Urbana-Champaign, Urbana, IL
21 61801, USA

22 *These authors contributed equally to this work.

23 §Correspondence: nicwu@illinois.edu (N.C.W.)

24 **ABSTRACT**

25 In the past two years, the global research in combating COVID-19 pandemic has led to isolation
26 and characterization of numerous human antibodies to the SARS-CoV-2 spike. This enormous
27 collection of antibodies provides an unprecedented opportunity to study the antibody response to
28 a single antigen. From mining information derived from 88 research publications and 13 patents,
29 we have assembled a dataset of ~8,000 human antibodies to the SARS-CoV-2 spike from >200
30 donors. Analysis of antibody targeting of different domains of the spike protein reveals a number
31 of common (public) responses to SARS-CoV-2, exemplified via recurring IGHV/IGK(L)V pairs,
32 CDR H3 sequences, IGHD usage, and somatic hypermutation. We further present a proof-of-
33 concept for prediction of antigen specificity using deep learning to differentiate sequences of
34 antibodies to SARS-CoV-2 spike and to influenza hemagglutinin. Overall, this study not only
35 provides an informative resource for antibody and vaccine research, but fundamentally advances
36 our molecular understanding of public antibody responses to a viral pathogen.

37 **INTRODUCTION**

38 From the beginning of COVID-19 pandemic, many research groups worldwide turned their
39 attention to SARS-CoV-2 and, in particular, to the immune response to infection and vaccination.
40 Over the past two years, thousands of human monoclonal antibodies to SARS-CoV-2 have been
41 isolated and characterized [1, 2]. The major surface antigen to which antibodies are elicited is the
42 SARS-CoV-2 spike (S) protein, which is a homotrimeric glycoprotein that facilitates virus entry by
43 first engaging the host receptor ACE2 and then mediating membrane fusion [3, 4]. The S protein
44 has three major domains, namely the N-terminal domain (NTD), receptor-binding domain (RBD),
45 and S2 domain [5, 6]. Most studies on SARS-CoV-2 antibodies have focused on the
46 immunodominant RBD [7], because neutralizing antibodies can be elicited to it with very high
47 potency [8, 9]. Antibodies to the NTD and the highly conserved S2 domain have also been
48 discovered, but usually exhibit lower neutralizing potency [10-16].

49

50 A common or public antibody response describes antibodies to the same antigen in different
51 donors that share genetic elements that usually result in similar modes of antigen recognition.
52 Deciphering public responses to particular antigens is not only critical for uncovering the
53 molecular features of recurring antibodies within the diverse antibody repertoire at the population
54 level, but also important for development of effective vaccines [17, 18]. A conventional approach
55 to study public antibody responses is to identify public clonotypes, which are antibodies from
56 different donors that share the same immunoglobulin heavy variable (IGHV) gene and with similar
57 complementarity-determining region (CDR) H3 sequences [19-23]. While this definition of public
58 clonotypes has improved our understanding of public antibody response, it generally ignores the
59 contribution of the light chain. Moreover, our recent study has shown that a public antibody
60 response to influenza hemagglutinin is driven by an IGHD gene with minimal dependence on the
61 IGHV gene [24]. Therefore, the true extent and molecular characterization of public antibody
62 responses remain to be explored.

63

64 Although information of many human clonal antibodies to SARS-CoV-2 is now publicly available,
65 it has been difficult to leverage all available information to investigate public antibody responses
66 to SARS-CoV-2. One major challenge is that the data from different studies are rarely in the same
67 format. This inconsistency imposes a huge barrier to data mining. The establishment of the
68 coronavirus antibody database (CoV-AbDab) has enabled researchers to deposit their antibody
69 data in a standardized format and has partially resolved the data formatting issue [2]. However,
70 not every SARS-CoV-2 antibody study has deposited their data to CoV-AbDab. Furthermore,
71 IGHD gene identities, nucleotide sequences, and donor IDs are not available in CoV-AbDab,
72 which makes it challenging to study public antibody responses using CoV-AbDab. Thus,
73 additional efforts must be made to fully synergize the information across many different SARS-
74 CoV-2 antibody studies to investigate and decipher public antibody responses.

75

76 In this study, we performed a systematic literature survey and assembled a large dataset of
77 human SARS-CoV-2 monoclonal antibodies with donor information. We then analyzed this
78 dataset and uncovered many previously unknown antibody sequence features that contribute to
79 public antibody responses to SARS-CoV-2 S. For example, we identified a public antibody
80 response to RBD that is largely independent of the IGHV gene, as well as involvement of a
81 particular IGHD gene in a public antibody response to S2. Our analysis also revealed a number
82 of recurring somatic hypermutations (SHMs) in different public clonotypes.

83

84 **RESULTS**

85 **Collection of SARS-CoV-2 antibody information**

86 Information for 8,048 human antibodies was collected from 88 research publications and 13
87 patents that described the discovery and characterization of antibodies to SARS-CoV-2 (**Figure**
88 **S1, Data S1**). Among these antibodies, which were isolated from 215 different donors, 7,997

89 (99.4%) react with SARS-CoV-2, and the remaining 51 react with SARS-CoV or seasonal
90 coronaviruses. While 99.1% (7,923/7,997) SARS-CoV-2 antibodies in our dataset bind to S
91 protein, 49 bind to N and 25 to ORF8. Epitope information was available for most SARS-CoV-2 S
92 antibodies, with 5,002 to RBD, 513 to NTD, and 890 to S2. In addition, information on
93 neutralization activity, germline gene usage, sequence, structure, bait for isolation (e.g. RBD, S),
94 and donor status (e.g. infected patient, vaccinee, etc.), if available, was collected for individual
95 antibodies.

96

97 **Epitope-dependent V gene usage bias in SARS-CoV-2 S antibodies**

98 To identify the sequence features in RBD, NTD, and S2 antibodies, we first performed an analysis
99 on V gene usage. Our analysis identified several commonly used IGHV/IGK(L)V pairs among
100 RBD antibodies (**Figure 1A**), such as IGHV3-53/IGKV1-9 and IGHV3-53/IGKV3-20, which
101 represent two known public clonotypes [25-30]. We also observed substantial enrichment of
102 IGHV1-24 among NTD antibodies over the naïve baseline (**Figure 1B**), which was established by
103 published datasets of antibody repertoire sequencing from 26 healthy donors [31-33]. IGHV1-24
104 is in fact a known public antibody response that targets an antigenic supersite on NTD [10-13].
105 These observations illustrate that the gene usage pattern in our dataset is consistent with previous
106 findings. Importantly, our dataset also enabled us to discover previously unknown patterns in gene
107 usage. For example, IGHV3-30 and IGHV3-30-3 were highly enriched among S2 antibodies over
108 baseline (**Figure 1B**). For our subsequent analyses, IGHV3-30-3 was also labeled as IGHV3-30,
109 since IGHV3-30 and IGHV3-30-3 have an identical amino acid sequence in the framework
110 regions, CDR H1 and CDR H2. V gene usage bias was also observed in the light chain. For
111 example, IGKV3-20 and IGKV3-11 were most used among S2 antibodies, whereas IGKV1-33
112 and IGKV1-39 were most used among RBD antibodies (**Figure 1C**). Overall, these results
113 demonstrated that RBD, NTD, and S2 antibodies have distinct patterns of V gene usage.

114

115 **CDR H3 analysis reveals public antibody response**

116 Although heavy and light chain V genes together encode four of the six CDRs, most of the
117 antibody sequence diversity comes from the CDR H3 region due to V(D)J recombination. Since
118 CDR H3 is typically an important determinant for binding and may even dominate the paratope
119 [24, 34-37], characterization of CDR H3 sequences in S antibodies is essential for understanding
120 the antibody response to SARS-CoV-2. Here, we aimed to examine the convergence of CDR H3
121 sequences among S antibodies. Briefly, CDR H3 sequences with the same length were clustered
122 by an 80% sequence identity cutoff. Only those clusters that contained antibodies from at least
123 two different donors were subjected to further analysis. A total of 170 clusters were identified
124 (**Figure 2A and Data S1**). Interestingly, antibodies within the same cluster often share the same
125 binding region on the S protein (RBD, NTD, or S2), consistent with the notion that the CDR H3
126 sequence has a critical role in determining the epitope that is recognized.

127

128 The largest cluster (cluster 1) consisted of 139 antibodies from 57 donors (**Figure 2B**). Most of
129 the antibodies in cluster 1 belonged to a well-characterized public clonotype to RBD that is
130 encoded by IGHV3-53/3-66 and IGKV1-9 [25-27, 29, 30]. IGHV3-53/3-66, which is frequently
131 used in RBD antibodies [28], was also enriched among antibodies in several other major CDR H3
132 clusters (e.g. clusters 2, 4, 8, and 14). Antibodies that bind to quaternary epitopes by bridging two
133 RBDs on the same spike are found in clusters 14 and 17 [38] (**Figure S2**). Notably, both clusters
134 3 and 5, which target the RBD, contained a conserved disulfide bond (**Figure 2B**). Cluster 3
135 represents another well-characterized public clonotype that is encoded by IGHV1-58/IGKV3-20
136 [8, 9, 39, 40]. On the other hand, antibodies in cluster 5, which are largely encoded by IGHV3-
137 30/IGKV1-33, have not been extensively studied. Most antibodies within cluster 5 had relatively
138 weak neutralizing activity, if any, despite having reasonable binding affinity (**Table S1**). This result
139 suggests the existence of an RBD-targeting public clonotype that had minimal neutralizing activity.

140 Similar observation was made with RBD antibodies encoded by IGHV3-13/IGKV1-39, although
141 most of these antibodies did not share a similar CDR H3 (**Figure S3 and Table S2**).

142
143 Furthermore, we also discovered several S2-specific CDR H3 clusters (clusters 6, 9, and 11) that
144 were predominantly encoded by IGHV3-30 with diverse IGK(L)V genes, suggesting a public
145 heavy chain response to S2 (**Figure 2B**). Clusters 10 and 15 were also of interest to us. Cluster
146 10 was featured by a very short CDR H3 (6 amino acids, IMGT numbering) and was encoded by
147 IGHV4-59/IGKV3-20, which was a frequent V gene pair among the S2 antibodies. Cluster 15 was
148 encoded by IGHV1-69/IGKV3-11, which was the most used V gene pair among the S2 antibodies.
149 Therefore, clusters 10 and 15 represented two major S2 public clonotypes, despite their minimal
150 neutralizing activity (**Table S1**). In contrast to RBD- and S2-specific clusters, all NTD-specific CDR
151 H3 clusters had a relatively small size (**Figure 2A**), suggesting that the paratopes for most NTD
152 antibodies are not dominated by CDR H3.

153
154 **A public antibody response dominated by the light chain and CDR H3**
155 While most clusters have a dominant IGHV gene, diverse IGHV genes were observed in cluster
156 7 (**Figure 2B-C**). Most antibodies (42 out of 45) in cluster 7 used IGLV6-57, suggesting their
157 paratopes are mainly composed of CDR H3 and light chain. S2A4, which is encoded by IGHV3-
158 7/IGLV6-57 [41], is an antibody in cluster 7. A previously determined structure of S2A4 in complex
159 with RBD indeed demonstrates that its CDR H3 contributes 38% of the buried surface area (BSA)
160 of the epitope, whereas the light chain contributes 53% (**Figure 2D-E**). Specifically, IGLV6-57
161 forms an extensive H-bond network with the RBD (**Figure 2F**), whereas a ⁹⁷WLRG¹⁰⁰ motif at the
162 tip of CDR H3 interacts with the RBD through H-bonds, π - π stacking, and hydrophobic
163 interactions (**Figure 2G**). Although G100 does not participate in binding, it exhibits backbone
164 torsion angles ($\Phi = -94^\circ$, $\Psi = -160^\circ$) that are in the preferred region of Ramachandran plot for
165 glycine, but in the allowed region for non-glycine (**Figure S4**). Consistently, this ⁹⁷WLRG¹⁰⁰ motif

166 is highly conserved in cluster 7 (**Figure 2B**). These results illustrate that our CDR H3 clustering
167 analysis not only captured existing knowledge about public SARS-CoV-2 antibody responses, but
168 was able to uncover recurring sequence features among SARS-CoV-2 antibodies that were
169 previously unknown.

170

171 **IGHV3-30/IGHD1-26 is a recurring feature in S2 antibodies**

172 As a major contributor to CDR H3, the IGHD gene can also drive a public antibody response [24].
173 Consequently, we aimed to understand if there are any signature IGHD genes in SARS-CoV-2 S
174 antibodies. While the frequency of most IGHD genes were within the baseline level, IGHD1-26
175 was highly enriched among S2 antibodies (**Figure 3A**). These IGHD1-26 S2 antibodies were
176 predominantly encoded by IGHV3-30 (**Figure 3B**), which is one of the most used IGHV genes
177 among S2 antibodies (**Figure 1B**). In contrast, the IGK(L)V gene usage was more diverse among
178 these IGHD1-26 S2 antibodies, although several were more frequently used than others (**Figure**
179 **3C**), implying that this public antibody response to S2 is mainly driven by the heavy chain.
180 Interestingly, 70% of these IGHD1-26 S2 antibodies had a CDR H3 of 14 amino acids, whereas
181 only <20% of other S antibodies had a CDRH3 of 14 amino acids (**Figure 3D**). In fact, most
182 members of clusters 6, 9, and 11 in our CDR H3 analysis above (**Figure 2B**) represented this
183 public antibody response to S2. While CDR H3 is also encoded by the IGHJ gene, the distribution
184 of IGHJ gene usage in these IGHD1-26 S2 antibodies did not show a strong deviation from that
185 of other S antibodies in our dataset (**Figure 3E**).

186

187 In our dataset, there were 110 IGHD1-26 S2 antibodies from 17 donors with a CDR H3 length of
188 14 amino acids. Sequence logo analysis of these 110 antibodies revealed a conserved
189 ⁹⁷[S/G]G[S/N]Y¹⁰⁰ motif in the middle of their CDR H3 sequences (**Figure 3F**). In-depth analysis
190 of the CDR H3 sequences from three representative IGHD1-26 S2 antibodies, namely P008_088,
191 G32M4, and ADI-56059, further indicated that the conserved ⁹⁷[S/G]G[S/N]Y¹⁰⁰ motif was within

192 the IGHD1-26-encoded region (**Figure 3G**). Of note, P008_088, G32M4, and ADI-56059 were
193 isolated from three different donors by three independent research groups [42-44]. While
194 P008_088 and G32M4 were from SARS-CoV-2 infected individuals, ADI-56059 was from a
195 SARS-CoV survivor. Although 87 out of these 110 IGHD1-26 S2 antibodies can cross-react with
196 SARS-CoV, they generally have minimal neutralization activity (**Table S3**). Together, these
197 results show that IGHV3-30/IGHD1-26 represents a public antibody response to a highly
198 conserved epitope in S2.

199

200 **Recurring somatic hypermutations in public antibody responses**

201 Our recent study has shown that V_H Y58F is a recurring somatic hypermutation (SHM) among
202 IGHV3-53 antibodies to SARS-CoV-2 RBD [25]. Here, we aimed to identify additional recurring
203 SHMs in other public clonotypes to SARS-CoV-2 S. In this analysis, antibodies from at least two
204 donors that had the same IGHV/IGK(L)V genes and CDR H3s from the same CDR H3 cluster
205 were classified as a public clonotype (**Figure 4A**). SHM that occurred in at least two donors within
206 a public clonotypes was defined as a recurring SHM. Our analysis here only focused on major
207 public clonotypes with antibodies from at least nine donors. This analysis led to the identification
208 of several recurring SHMs in IGHV3-53/3-66-encoded public clonotypes that were previously
209 characterized, including V_H F27V, T28I, and Y58F [25, 45, 46] (**Figure S5**). We also identified
210 many other previously unknown recurring SHMs in both heavy and light chains (**Figure 4A-B**),
211 including V_L S29R in a IGHV1-58/IGKV3-20 public clonotype that belongs to cluster 3 of our CDR
212 H3 clustering analysis (**Figure 2A-B**). V_L S29R emerged in 8 out of 26 (31%) donors that carried
213 this IGHV1-58/IGKV3-20 public clonotype.

214

215 Antibodies of this IGHV1-58/IGKV3-20 public clonotype bind to the ridge region of SARS-CoV-2
216 RBD (**Figure 5A**), and can be robustly elicited by infection with antigenically distinct variants of
217 SARS-CoV-2 [39, 47] and by vaccination [48, 49]. These antibodies are also able to potently

218 neutralize multiple variants of concern (VOC) [9, 48, 50]. We compared two previously determined
219 structures of IGHV1-58/IGKV3-20 antibodies in complex with RBD [40, 51], where one has the
220 germline-encoded V_L S29 (**Figure 5B**) and the other carries a somatically mutated V_L R29 (**Figure**
221 **5C**). While neither V_L S29 nor V_L R29 directly interact with RBD, V_L R29 is able to form a cation-
222 π interaction with V_L Y32, which in turn forms a T-shaped π-π stacking with RBD-F486 and H-
223 bonds with RBD-C480 (**Figure 5C**). In the absence of SHM V_L S29R, the rotamer adopted by V_L
224 Y32 does not permit these interactions to be formed. During our structural analysis, we discovered
225 that V_L S29R forms a salt bridge with another SHM V_L G92D (**Figure 5C**), which can further
226 stabilize the interactions between V_L Y32 and with RBD. In fact, it is likely that V_L S29R promoted
227 the emergence of V_L G92D, since V_L G92D was found in four out of the 67 antibodies and all four
228 that carried V_L S29R (**Figure 5D-E**). This analysis substantiates the notion that recurring SHM
229 can be found among antibodies within a public clonotype and further suggests the existence of
230 common affinity maturation pathways that involve emergence of multiple SHMs in a defined order.
231

232 **Antigen identification by deep learning**

233 Since many sequence features of public antibody responses to the S protein can be observed in
234 our dataset, we postulated that the dataset is sufficiently large to train a deep learning model to
235 identify S antibodies. To provide a proof-of-concept, we aimed to train a deep learning model to
236 distinguish between antibodies to S and to influenza hemagglutinin (HA). Among different
237 antigens, HA was chosen here because there are a large number of HA antibodies with published
238 sequences, albeit still lower than the published SARS-CoV-2 S antibodies. Here, 4,736 unique
239 SARS-CoV-2 S antibodies and 2,204 unique influenza HA antibodies with complete information
240 for all six CDR sequences were used (**Data S2**). Sequences for HA antibodies were retrieved
241 from GenBank [52]. None of these antibodies have identical sequences in all six CDRs. These
242 antibodies to S and HA were divided into a training set (64%), a validation set (16%), and a test
243 set (20%), with no overlap between the three sets. The training set was used to train the deep

244 learning model. The validation set was used to evaluate the model performance during training.

245 The test set was used to evaluate the performance of the final model.

246

247 Our deep learning model has a simple architecture, which consisted of one encoder per CDR

248 followed by three fully connected layers (**Figure 6A**). To evaluate the model performance on the

249 test set, the area under the curves of receiver operating characteristic (ROC AUC) and precision-

250 recall (PR AUC) were used to measure the model's ability to avoid misclassification. While ROC

251 AUC is popular evaluation metric [53], PR AUC is shown to be more informative for evaluating

252 models that are trained with imbalanced datasets [54]. Model performance was the best when all

253 six CDRs (i.e. H1, H2, H3, L1, L2, and L3) were used to train the model, which resulted in an

254 ROC AUC and an PR AUC of 0.87 and 0.92, respectively (**Figure 6B and Table S4**). Interesting,

255 a similar performance was observed when the model was trained by the three heavy-chain CDRs

256 (i.e. H1, H2, and H3) (ROC AUC = 0.86, PR AUC = 0.91), indicating that the heavy chain

257 sequence captures most of the information to distinguish between HA antibodies and S

258 antibodies. A reasonable performance was also observed when the model was trained by the

259 three light-chain CDRs (i.e. L1, L2, and L3) (ROC AUC = 0.77, PR AUC = 0.86). For other types

260 of inputs that we have tested, including CDR H3 only, CDR L3 only, CDR H3+L3, CDR H1+H2,

261 and CDR L1+L2, the ROC AUCs were between 0.72 and 0.83 and the PR AUCs were between

262 0.82 and 0.90. These results imply that IGHV-encoded region (H1+H2), IGK(L)V-encoded region

263 (L1+L2), and the V(D)J junctions (CDR H3 and CDR L3) are all informative for predicting antigen

264 specificity. Overall, while our deep learning model had a relatively simple architecture, it was able

265 to discriminate between antibodies to two different antigens based on primary sequences.

266

267 A recent study reported 81 antibodies to SARS-CoV-2 RBD that were elicited by Beta variant

268 infection [47]. While these 81 antibodies were not included in the dataset that we assembled (**Data**

269 **S1**), they provided an opportunity to further evaluate the performance of our deep learning model.

270 Our deep learning model that was trained by all six CDRs (see above) successfully predicted that
271 72 of the 81 (89%) antibodies as SARS-CoV-2 S antibodies (**Figure 6C and Table S5**). This
272 result further demonstrates the possibility of predicting antibody specificity solely based on the
273 primary sequence.

274

275 **DISCUSSION**

276 Through a systematic survey of published information on SARS-CoV-2 antibodies, we identified
277 many molecular features of public antibody responses to SARS-CoV-2. The large amount of
278 published information has allowed us to explore distinct patterns of germline gene usages in
279 antibodies that target different domains on the S protein (i.e. RBD, NTD, and S2). Notably, the
280 types and nature of public antibody responses to different domains appear to be quite different.
281 For example, convergence of CDR H3 sequences can be readily identified in the public antibody
282 responses to RBD and S2. In contrast, the public antibody response to NTD seems to be largely
283 independent of the CDR H3 sequence. Furthermore, an IGHD-dependent public antibody
284 response was enriched against S2, but not RBD or NTD. Together, our study demonstrates the
285 diversity of sequence features that can constitute a public antibody response against a single
286 antigen.

287

288 The public antibody response to SARS-CoV-2 has also been examined by a recent data mining
289 study that focused on identifying public clonotypes [55]. This previous study defined public
290 clonotypes as antibodies with the same IGHV/IGHJ/IGK(L)V/IGK(L)V genes and high similarity of
291 CDR H3 [55]. While multiple public clonotypes were identified using this stringent definition [55],
292 the characterization of public antibody response is likely far from comprehensive. A public
293 antibody response may not always involve a defined pair of IGHV/IGK(L)V genes, especially when
294 either IGHV or IGK(L)V gene-encoded residues only make a minimal contribution to the paratope.
295 In fact, a well-characterized public antibody response to the highly conserved stem region of

296 influenza hemagglutinin has a paratope that is entirely attributed to the IGHV1-69 heavy chain
297 [56-59]. IGHV3-30/IGHD1-26 antibodies to S2 in our study may represent a similar type of
298 IGK(L)V-independent public antibody response, although it still needs to be confirmed by
299 structural analysis. On the other extreme, RBD antibodies that are encoded by IGLV6-57 with a
300 ⁹⁷WLRG¹⁰⁰ motif in the CDR H3 represent a public response that is largely independent of IGHV
301 gene usage. Given the diverse types of public antibody responses to SARS-CoV-2 S, we need to
302 acknowledge the limitation of using the conventional strict definition of public clonotype to study
303 public antibody responses.

304

305 Public antibody response to different antigens can have very different sequence features. For
306 example, IGHV6-1 and IGHD3-9 are signatures of public antibody response to influenza virus [24,
307 60-62], whereas IGHV3-23 is frequently used in antibodies to Dengue and Zika viruses [63]. In
308 contrast, these germline genes are seldom used in the antibody response to SARS-CoV-2 as
309 compared to the naïve baseline (**Figure 1B-C and Figure 3A**). Since the binding specificity of an
310 antibody is determined by its structure, which in turn is determined by its amino acid sequence,
311 the antigen specificity of an antibody can theoretically be identified based on its sequence. This
312 study provides a proof-of-concept by training a deep learning model to distinguish between SARS-
313 CoV-2 S antibodies and influenza HA antibodies, solely based on primary sequence information.
314 Technological advancements, such as the development of single-cell high-throughput screen
315 using the Berkeley Lights Beacon optofluidics device [64] and advances in paired B-cell receptor
316 sequencing [65], have been accelerating the speed of antibody discovery and characterization.
317 As more sequence information on antibodies to different antigens is accumulated, we may be
318 able in the future to construct a generalized sequence-based model to accurately predict the
319 antigen specificity of any antibody.

320

321 In summary, the amount of publicly available information on SARS-CoV-2 antibodies has provided
322 invaluable biological insights that have not been readily obtained for other pathogens. One reason
323 is that the COVID-19 pandemic has gathered scientists from many fields and around the globe to
324 work intensively on SARS-CoV-2. The parallel efforts by many different research groups have
325 enabled SARS-CoV-2 antibodies to be discovered in unprecedented speed and scale that have
326 not been possible for other pathogens. We anticipate that knowledge of the molecular features of
327 the antibody response to SARS-CoV-2 will keep accumulating as more antibodies are isolated
328 and characterized. Ultimately, the extensive characterization of antibodies to the SARS-CoV-2 S
329 protein may allow us to address some of the most fundamental questions about antigenicity and
330 immunogenicity, as well as how the human immune repertoire has evolved to respond to specific
331 classes of viral pathogens that have coexisted with humans for hundreds to thousands of years.

332

333 **MATERIALS AND METHODS**

334 **Collection of antibody information**

335 Information on the monoclonal antibodies is derived from the original papers (Supplementary
336 Table 1). Sequences of each monoclonal antibody are from the original papers and/or NCBI
337 GenBank database (www.ncbi.nlm.nih.gov/genbank) [52]. Putative germline genes were
338 identified by IgBLAST [66]. Some studies isolated antibodies from multiple donors, but the donor
339 identity for each antibody was not always clear. For example, some studies mixed B cells from
340 multiple donors before isolating individual B cell clones. Since the donor identity cannot be
341 distinguished among those antibodies, we considered them from the same donor with “_mix” as
342 the suffix of the donor ID. In addition, the PBMCs of SARS-CoV survivors in three separate studies
343 were all from NIH/VRC [12, 44, 67]. Since it is unclear if they are the same SARS-CoV survivor,
344 the same donor ID “VRC_SARS1” was assigned to them to avoid overestimation of public
345 antibody response. the neutralization activity of a given antibody was only measured at a single
346 concentration, 50% neutralization activity or below was classified as non-neutralizing. We also

347 downloaded the CoV-AbDab [2] in September 2021 to fill in any additional information. As of
348 September 2021, there were 2,582 human SARS-CoV-2 antibodies in CoV-AbDab. Information
349 in the finalized dataset was manually inspected by three different individuals. For antibodies that
350 were shown to bind to S1 but not RBD, they were classified as NTD antibodies. Due to having
351 identical nucleotide sequences, IGKV1D-39*01 was classified as IGKV1-39*01, IGHV1-68D*02
352 as IGHV1-68*02, IGHV1-69D*01 as IGHV1-69*19, IGHV3-23D*01 as IGHV3-23*01, and IGHV3-
353 29*01 as IGHV3-30-42*01.

354

355 **Analysis of germline gene usages**

356 Non-functional germline genes were ignored in our germline gene usage analysis. Except for the
357 analysis presented in **Figure 1**, IGHV3-30-3 was classified as IGHV3-30 since they have identical
358 amino-acid sequence in the framework regions, CDR H1, and CDR H2. To establish the baseline
359 germline usage frequency, published antibody repertoire sequencing datasets from 26 healthy
360 donors [31, 32] were downloaded from cAb-Rep [33]. Putative germline genes for each antibody
361 sequence in these repertoire sequencing datasets from healthy donors were identified by were
362 identified by IgBLAST [66].

363

364 **CDR H3 clustering analysis**

365 Using a deterministic clustering approach, antibodies with CDR H3 sequences that had the same
366 length and at least 80% amino-acid sequence identity were assigned to the same cluster. As a
367 result, CDR H3 of every antibody in a cluster would have >20% difference in amino-acid sequence
368 identity with that of every antibody in another cluster. A cluster would be discarded if all of its
369 antibody members were from the same donor. The number of antibodies within a cluster was
370 defined as the cluster size. Sequence logos were generated by Logomaker in Python [68]. For
371 each cluster, epitope assignment was performed using the following scoring scheme. Briefly,
372 there were three scoring categories, namely “RBD”, “NTD”, and “S2”.

373 • 1 point was added to category “RBD” for each antibody with an epitope label equals to
374 “S:RBD” or “S:S1”.

375 • 1 point was added to category “NTD” for each antibody with an epitope label equals to
376 “S:NTD”, “S:S1”, “S:non-RBD”, or “S:S1 non-RBD”.

377 • 1 point was added to category “S2” for each antibody with an epitope label equals to
378 “S:S2”, “S:S2 Stem Helix”, “S:non-RBD”.

379 The category with >50% of the total points would be classified as the epitope for a given cluster.

380 If no category had >50% of the total points, the epitope for the cluster would be classified as
381 “unknown”.

382

383 **Identification of recurring somatic hypermutation (SHM)**

384 In this study, a public clonotype was classified as antibodies from at least two donors that had the
385 same IGHV/IGK(L)V genes and CDR H3s from the same CDR H3 cluster (see “CDR H3 clustering
386 analysis” above). For each antibody, ANARCI was used to number the position of each residue
387 according to Kabat numbering [69]. The amino-acid identity at each residue position of an
388 antibody was then compared to that of the putative germline gene. CDR H3, CDR L3, and
389 framework region 4 in both heavy and light chains were not included in this analysis. Insertions
390 and deletions were also ignored in this analysis. SHM that occurred in at least two donors within
391 a public clonotype was defined as a recurring SHM.

392

393 **Deep learning model for antigen identification**

394 Model construction

395 The deep learning model consisted of two networks, namely multi-encoder (ME) and a stack of
396 multi-layered perceptrons (MLP). The CDR amino-acid sequences were taken as input and
397 passed to ME. Specifically, each CDR amino-acid sequence was described by a 21-letter
398 alphabet vector $\vec{x} = (x_1, x_2, \dots, x_{L-1}, x_L), x \in \mathbb{R}^L$, where L represented the length of sequence, and

399 x represented the amino acid category. Each of the 20 canonical amino acids was one category,
400 whereas all the ambiguous amino acids were grouped as the 21st category. Before passing to
401 ME, inputs were tokenized at the amino-acid level and processed by zero padding, so that the
402 embedding layers represented the character-level tokens (i.e. amino acids) and the size of each
403 input was the same. Subsequently, the inputs were mapped to the embedding vectors with
404 additional dimension d . The sinusoidal positional encoding vectors were added to the embedding
405 vectors to encode the relative position of tokens (i.e. amino acids) in the sequence. Each
406 embedding vector, $\vec{x} \in \mathbb{R}^{L \times d}$, with size of $L \times d$, was passed into transformer encoder layer by
407 self-attention mechanism to learn the sequence feature [70]. All learned sequence features were
408 then concatenated together and passed to multi-layered perceptron (MLP). Each MLP layer
409 contained leaky rectified linear unit (ReLU) activations to avoid the vanishing gradient. Dropout
410 layers were placed after each MLP block to avoid model overfitting [71]. The final output layer
411 was followed by a sigmoid activation function to predict the probability of different classes. The
412 prediction losses were calculated by binary cross-entropy loss.

413

414 Training detail

415 SARS-CoV-2 S antibodies and influenza HA antibodies with complete information for all six CDR
416 sequences were identified. Sequences of each antibody were from the original papers (**Data S2**)
417 or NCBI GenBank database (www.ncbi.nlm.nih.gov/genbank) [52]. If all six CDR sequences were
418 the same between two or more antibodies, only one of these antibodies would be retained. After
419 filtering duplicates, there were 4,736 antibodies to SARS-CoV-2 and 2,204 to influenza HA. The
420 CDR sequences were identified by IgBLAST and PyIR [66, 72]. This dataset was randomly split
421 into a training set (64%), a validation set (16%), and a test set (20%). The training set was used
422 to train the deep learning model. The validation set was used to evaluate the model performance
423 during training. The test set was used to evaluate the performance of the final model. There was
424 no overlap of antibody sequences among the training set, validation set, and test set. The Adam

425 algorithm was used to optimize the model. The following hyper-parameters were used for model
426 training:

427 • CDR embedding size: 256
428 • The number of attention heads for self-attention on CDR feature learning: 4
429 • The number of encoder layer for CDR encoder: 4
430 • Size of stacking MLP layers: 512, 128, and 64
431 • Learning rate: 0.0001
432 • Batch size: 256

433

434 Using the same training set, validation set and test set, the model performance of using the
435 following inputs was compared:

436 1. CDR H1 + H2
437 2. CDR L1 + L2
438 3. CDR H3
439 4. CDR L3
440 5. CDR H3 + L3
441 6. CDR H1 + H2 + H3
442 7. CDR L1 + L2 + L3
443 8. CDR H1 + H2 + H3 + L1 + L2 + L3

444

445 Performance Metrics

446 For evaluating model performance, S antibodies and HA antibodies were considered “positive”
447 and “negative”, respectively. False positives (FP) and false negatives (FN) were samples that
448 were misclassified by the model while true negatives (TN) and true positives (TP) were correctly
449 classified one. The following metrics were computed to evaluate model performance:

450
$$accuracy = \frac{TP + TN}{TP + FN + FP + TN} \quad (1)$$

451
$$precision = \frac{TP}{TP + FP} \quad (2)$$

452
$$recall = \frac{TP}{TP + FN} \quad (3)$$

453 In addition, we also used the receiver operating characteristic (ROC) curve and precision-recall
454 (PR) curve to measure the model's ability to avoid misclassification [53, 54]. Area under the curves
455 of ROC (i.e. ROC AUC) and PR (i.e. PR AUC) were computed using the "keras.metrics" module
456 in TensorFlow [73].

457

458 **DATA AVAILABILITY**

459 The assembled SARS-CoV-2 antibody dataset is in **Data S1**. The dataset for constructing and
460 testing the deep learning model is in **Data S2**.

461

462 **CODE AVAILABILITY**

463 Custom python scripts for all analyses have been deposited to <https://github.com/nicwulab/SARS->
464 [CoV-2_Abs.](#)

465

466 **ACKNOWLEDGEMENT**

467 This work was supported by National Institutes of Health (NIH) R00 AI139445 (N.C.W.), DP2
468 AT011966 (N.C.W.), and Bill and Melinda Gates Foundation INV-004923 (I.A.W.). We thank Seth
469 Zost and Huibin Lv for helpful discussion.

470

471 **AUTHOR CONTRIBUTIONS**

472 All authors conceived and designed the study. Y.W, M.Y. and N.C.W. assembled the dataset and
473 performed data analysis. J.P. provided technical expertise in deep learning, Y.W., M.Y. I.A.W,
474 and N.C.W. wrote the paper and all authors reviewed and/or edited the paper.

475

476 REFERENCES

- 477 1. Li D, Sempowski GD, Saunders KO, Acharya P, Haynes BF. SARS-CoV-2 neutralizing
478 antibodies for COVID-19 prevention and treatment. *Annu Rev Med*. 2021. Epub
479 2021/08/25. doi: 10.1146/annurev-med-042420-113838. PubMed PMID: 34428080.
- 480 2. Raybould MJ, Kovaltsuk A, Marks C, Deane CM. CoV-AbDab: the coronavirus antibody
481 database. *Bioinformatics*. 2021;37(5):734-5. Epub 2020/08/18. doi:
482 10.1093/bioinformatics/btaa739. PubMed PMID: 32805021; PubMed Central PMCID:
483 PMCPMC7558925.
- 484 3. Zhou P, Yang XL, Wang XG, Hu B, Zhang L, Zhang W, et al. A pneumonia outbreak
485 associated with a new coronavirus of probable bat origin. *Nature*. 2020;579(7798):270-3.
486 Epub 2020/02/06. doi: 10.1038/s41586-020-2012-7. PubMed PMID: 32015507.
- 487 4. Shang J, Wan Y, Luo C, Ye G, Geng Q, Auerbach A, et al. Cell entry mechanisms of
488 SARS-CoV-2. *Proc Natl Acad Sci U S A*. 2020;117(21):11727-34. Epub 2020/05/08. doi:
489 10.1073/pnas.2003138117. PubMed PMID: 32376634; PubMed Central PMCID:
490 PMCPMC7260975.
- 491 5. Walls AC, Park YJ, Tortorici MA, Wall A, McGuire AT, Veesler D. Structure, function,
492 and antigenicity of the SARS-CoV-2 spike glycoprotein. *Cell*. 2020;181(2):281-92.e6.
493 Epub 2020/03/11. doi: 10.1016/j.cell.2020.02.058. PubMed PMID: 32155444.
- 494 6. Wrapp D, Wang N, Corbett KS, Goldsmith JA, Hsieh CL, Abiona O, et al. Cryo-EM
495 structure of the 2019-nCoV spike in the prefusion conformation. *Science*.
496 2020;367(6483):1260-3. Epub 2020/02/23. doi: 10.1126/science.abb2507. PubMed
497 PMID: 32075877.
- 498 7. Yuan M, Liu H, Wu NC, Wilson IA. Recognition of the SARS-CoV-2 receptor binding
499 domain by neutralizing antibodies. *Biochem Biophys Res Commun*. 2021;538:192-203.
500 Epub 2020/10/19. doi: 10.1016/j.bbrc.2020.10.012. PubMed PMID: 33069360; PubMed
501 Central PMCID: PMCPMC7547570.
- 502 8. Tortorici MA, Beltramello M, Lempp FA, Pinto D, Dang HV, Rosen LE, et al. Ultrapotent
503 human antibodies protect against SARS-CoV-2 challenge via multiple mechanisms.
504 *Science*. 2020;370(6519):950-7. Epub 2020/09/26. doi: 10.1126/science.abe3354.
505 PubMed PMID: 32972994; PubMed Central PMCID: PMCPMC7857395.
- 506 9. Wang L, Zhou T, Zhang Y, Yang ES, Schramm CA, Shi W, et al. Ultrapotent antibodies
507 against diverse and highly transmissible SARS-CoV-2 variants. *Science*.
508 2021;373(6556):eab1766. Epub 2021/07/03. doi: 10.1126/science.abh1766. PubMed
509 PMID: 34210892.

510 10. Voss WN, Hou YJ, Johnson NV, Delidakis G, Kim JE, Javanmardi K, et al. Prevalent,
511 protective, and convergent IgG recognition of SARS-CoV-2 non-RBD spike epitopes.
512 *Science*. 2021;372(6546):1108-12. Epub 2021/05/06. doi: 10.1126/science.abg5268.
513 PubMed PMID: 33947773; PubMed Central PMCID: PMCPMC8224265.

514 11. Cerutti G, Guo Y, Zhou T, Gorman J, Lee M, Rapp M, et al. Potent SARS-CoV-2
515 neutralizing antibodies directed against spike N-terminal domain target a single
516 supersite. *Cell Host Microbe*. 2021;29(5):819-33.e7. Epub 2021/04/01. doi:
517 10.1016/j.chom.2021.03.005. PubMed PMID: 33789084; PubMed Central PMCID:
518 PMCPMC7953435.

519 12. Li D, Edwards RJ, Manne K, Martinez DR, Schafer A, Alam SM, et al. In vitro and in vivo
520 functions of SARS-CoV-2 infection-enhancing and neutralizing antibodies. *Cell*.
521 2021;184(16):4203-19.e32. Epub 2021/07/10. doi: 10.1016/j.cell.2021.06.021. PubMed
522 PMID: 34242577; PubMed Central PMCID: PMCPMC8232969.

523 13. Chi X, Yan R, Zhang J, Zhang G, Zhang Y, Hao M, et al. A neutralizing human antibody
524 binds to the N-terminal domain of the Spike protein of SARS-CoV-2. *Science*.
525 2020;369(6504):650-5. Epub 2020/06/24. doi: 10.1126/science.abc6952. PubMed PMID:
526 32571838; PubMed Central PMCID: PMCPMC7319273.

527 14. Zhou P, Yuan M, Song G, Beutler N, Shaabani N, Huang D, et al. A protective broadly
528 cross-reactive human antibody defines a conserved site of vulnerability on beta-
529 coronavirus spikes. *bioRxiv*. 2021. Epub 2021/04/07. doi: 10.1101/2021.03.30.437769.
530 PubMed PMID: 33821273; PubMed Central PMCID: PMCPMC8020973.

531 15. Pinto D, Sauer MM, Czudnochowski N, Low JS, Tortorici MA, Housley MP, et al. Broad
532 betacoronavirus neutralization by a stem helix-specific human antibody. *Science*.
533 2021;373(6559):1109-16. Epub 2021/08/05. doi: 10.1126/science.abj3321. PubMed
534 PMID: 34344823.

535 16. Li W, Chen Y, Prevost J, Ullah I, Lu M, Gong SY, et al. Structural basis and mode of
536 action for two broadly neutralizing antibodies against SARS-CoV-2 emerging variants of
537 concern. *bioRxiv*. 2021. Epub 2021/08/11. doi: 10.1101/2021.08.02.454546. PubMed
538 PMID: 34373853; PubMed Central PMCID: PMCPMC8351775.

539 17. Lanzavecchia A, Fruhwirth A, Perez L, Corti D. Antibody-guided vaccine design:
540 identification of protective epitopes. *Curr Opin Immunol*. 2016;41:62-7. Epub 2016/06/28.
541 doi: 10.1016/j.co.2016.06.001. PubMed PMID: 27343848.

542 18. Andrews SF, McDermott AB. Shaping a universally broad antibody response to influenza
543 amidst a variable immunoglobulin landscape. *Curr Opin Immunol*. 2018;53:96-101. doi:
544 10.1016/j.co.2018.04.009. PubMed PMID: 29730560.

545 19. Setliff I, McDonnell WJ, Raju N, Bombardi RG, Murji AA, Scheepers C, et al. Multi-donor
546 longitudinal antibody repertoire sequencing reveals the existence of public antibody
547 clonotypes in HIV-1 infection. *Cell Host Microbe*. 2018;23(6):845-54.e6. Epub
548 2018/06/05. doi: 10.1016/j.chom.2018.05.001. PubMed PMID: 29861170; PubMed
549 Central PMCID: PMCPMC6002606.

550 20. Jackson KJ, Liu Y, Roskin KM, Glanville J, Hoh RA, Seo K, et al. Human responses to
551 influenza vaccination show seroconversion signatures and convergent antibody
552 rearrangements. *Cell Host Microbe*. 2014;16(1):105-14. Epub 2014/07/02. doi:
553 10.1016/j.chom.2014.05.013. PubMed PMID: 24981332; PubMed Central PMCID:
554 PMC4158033.

555 21. Truck J, Ramasamy MN, Galson JD, Rance R, Parkhill J, Lunter G, et al. Identification of
556 antigen-specific B cell receptor sequences using public repertoire analysis. *J Immunol*.
557 2015;194(1):252-61. Epub 2014/11/14. doi: 10.4049/jimmunol.1401405. PubMed PMID:
558 25392534; PubMed Central PMCID: PMC4272858.

559 22. Henry Dunand CJ, Wilson PC. Restricted, canonical, stereotyped and convergent
560 immunoglobulin responses. *Philos Trans R Soc Lond B Biol Sci*.
561 2015;370(1676):20140238. Epub 2015/07/22. doi: 10.1098/rstb.2014.0238. PubMed
562 PMID: 26194752; PubMed Central PMCID: PMC4528415.

563 23. Pieper K, Tan J, Piccoli L, Foglierini M, Barbieri S, Chen Y, et al. Public antibodies to
564 malaria antigens generated by two LAIR1 insertion modalities. *Nature*.
565 2017;548(7669):597-601. Epub 2017/08/29. doi: 10.1038/nature23670. PubMed PMID:
566 28847005; PubMed Central PMCID: PMC5635981.

567 24. Wu NC, Yamayoshi S, Ito M, Uraki R, Kawaoka Y, Wilson IA. Recurring and adaptable
568 binding motifs in broadly neutralizing antibodies to influenza virus are encoded on the
569 D3-9 segment of the Ig gene. *Cell Host Microbe*. 2018;24(4):569-78.e4. doi:
570 10.1016/j.chom.2018.09.010. PubMed PMID: 30308159.

571 25. Tan TJC, Yuan M, Kuzelka K, Padron GC, Beal JR, Chen X, et al. Sequence signatures
572 of two public antibody clonotypes that bind SARS-CoV-2 receptor binding domain. *Nat
573 Commun*. 2021;12(1):3815. Epub 2021/06/23. doi: 10.1038/s41467-021-24123-7.
574 PubMed PMID: 34155209.

575 26. Cao Y, Su B, Guo X, Sun W, Deng Y, Bao L, et al. Potent neutralizing antibodies against
576 SARS-CoV-2 identified by high-throughput single-cell sequencing of convalescent
577 patients' B cells. *Cell*. 2020;182(1):73-84.e16. Epub 2020/05/20. doi:
578 10.1016/j.cell.2020.05.025. PubMed PMID: 32425270; PubMed Central PMCID:
579 PMC7231725.

580 27. Kim SI, Noh J, Kim S, Choi Y, Yoo DK, Lee Y, et al. Stereotypic neutralizing VH
581 antibodies against SARS-CoV-2 spike protein receptor binding domain in patients with
582 COVID-19 and healthy individuals. *Sci Transl Med*. 2021;13(578):eabd6990. Epub
583 2021/01/06. doi: 10.1126/scitranslmed.abd6990. PubMed PMID: 33397677; PubMed
584 Central PMCID: PMC7875332.

585 28. Yuan M, Liu H, Wu NC, Lee CD, Zhu X, Zhao F, et al. Structural basis of a shared
586 antibody response to SARS-CoV-2. *Science*. 2020;369(6507):1119-23. Epub
587 2020/07/15. doi: 10.1126/science.abd2321. PubMed PMID: 32661058; PubMed Central
588 PMCID: PMC7402627.

589 29. Clark SA, Clark LE, Pan J, Coscia A, McKay LGA, Shankar S, et al. SARS-CoV-2
590 evolution in an immunocompromised host reveals shared neutralization escape
591 mechanisms. *Cell*. 2021;184(10):2605-17.e18. Epub 2021/04/09. doi:

592 10.1016/j.cell.2021.03.027. PubMed PMID: 33831372; PubMed Central PMCID:
593 PMCPMC7962548.

594 30. Zhang Q, Ju B, Ge J, Chan JF, Cheng L, Wang R, et al. Potent and protective IGHV3-
595 53/3-66 public antibodies and their shared escape mutant on the spike of SARS-CoV-2.
596 Nat Commun. 2021;12(1):4210. Epub 2021/07/11. doi: 10.1038/s41467-021-24514-w.
597 PubMed PMID: 34244522; PubMed Central PMCID: PMCPMC8270942.

598 31. Soto C, Bombardi RG, Branchizio A, Kose N, Matta P, Sevy AM, et al. High frequency of
599 shared clonotypes in human B cell receptor repertoires. Nature. 2019;566(7744):398-
600 402. Epub 2019/02/15. doi: 10.1038/s41586-019-0934-8. PubMed PMID: 30760926;
601 PubMed Central PMCID: PMCPMC6949180.

602 32. Briney B, Inderbitzin A, Joyce C, Burton DR. Commonality despite exceptional diversity
603 in the baseline human antibody repertoire. Nature. 2019;566(7744):393-7. Epub
604 2019/01/22. doi: 10.1038/s41586-019-0879-y. PubMed PMID: 30664748; PubMed
605 Central PMCID: PMCPMC6411386.

606 33. Guo Y, Chen K, Kwong PD, Shapiro L, Sheng Z. cAb-Rep: a database of curated
607 antibody repertoires for exploring antibody diversity and predicting antibody prevalence.
608 Front Immunol. 2019;10:2365. Epub 2019/10/28. doi: 10.3389/fimmu.2019.02365.
609 PubMed PMID: 31649674; PubMed Central PMCID: PMCPMC6794461.

610 34. Liu H, Wu NC, Yuan M, Bangaru S, Torres JL, Caniels TG, et al. Cross-neutralization of
611 a SARS-CoV-2 antibody to a functionally conserved site is mediated by avidity.
612 Immunity. 2020;53(6):1272-80.e5. Epub 2020/11/27. doi: 10.1016/j.jimmuni.2020.10.023.
613 PubMed PMID: 33242394; PubMed Central PMCID: PMCPMC7687367 COVA1-16 and
614 other antibodies first disclosed by Brouwer et al. (2020) has been filed by Amsterdam
615 UMC under application number 2020-039EP-PR. I.A.W. is a member of the Immunity
616 Editorial Board.

617 35. Ekiert DC, Kashyap AK, Steel J, Rubrum A, Bhabha G, Khayat R, et al. Cross-
618 neutralization of influenza A viruses mediated by a single antibody loop. Nature.
619 2012;489(7417):526-32. doi: 10.1038/nature11414. PubMed PMID: 22982990; PubMed
620 Central PMCID: PMCPMC3538848.

621 36. Jette CA, Cohen AA, Gnanapragasam PNP, Muecksch F, Lee YE, Huey-Tubman KE, et
622 al. Broad cross-reactivity across sarbecoviruses exhibited by a subset of COVID-19
623 donor-derived neutralizing antibodies. Cell Rep. 2021;36(13):109760. Epub 2021/09/18.
624 doi: 10.1016/j.celrep.2021.109760. PubMed PMID: 34534459; PubMed Central PMCID:
625 PMCPMC84223902.

626 37. Pancera M, Changela A, Kwong PD. How HIV-1 entry mechanism and broadly
627 neutralizing antibodies guide structure-based vaccine design. Curr Opin HIV AIDS.
628 2017;12(3):229-40. Epub 2017/04/20. doi: 10.1097/COH.0000000000000360. PubMed
629 PMID: 28422787; PubMed Central PMCID: PMCPMC5557343.

630 38. Barnes CO, Jette CA, Abernathy ME, Dam KA, Esswein SR, Gristick HB, et al. SARS-
631 CoV-2 neutralizing antibody structures inform therapeutic strategies. Nature.
632 2020;588(7839):682-7. Epub 2020/10/13. doi: 10.1038/s41586-020-2852-1. PubMed
633 PMID: 33045718.

634 39. Robbiani DF, Gaebler C, Muecksch F, Lorenzi JCC, Wang Z, Cho A, et al. Convergent
635 antibody responses to SARS-CoV-2 in convalescent individuals. *Nature*. 2020;584:437-
636 42. doi: 10.1038/s41586-020-2456-9.

637 40. Dejnirattisai W, Zhou D, Ginn HM, Duyvesteyn HME, Supasa P, Case JB, et al. The
638 antigenic anatomy of SARS-CoV-2 receptor binding domain. *Cell*. 2021;184(8):2183-
639 200.e22. Epub 2021/03/24. doi: 10.1016/j.cell.2021.02.032. PubMed PMID: 33756110;
640 PubMed Central PMCID: PMCPMC7891125.

641 41. Piccoli L, Park YJ, Tortorici MA, Czudnochowski N, Walls AC, Beltramello M, et al.
642 Mapping neutralizing and immunodominant sites on the SARS-CoV-2 spike receptor-
643 binding domain by structure-guided high-resolution serology. *Cell*. 2020;183(4):1024-
644 42.e21. Epub 2020/09/30. doi: 10.1016/j.cell.2020.09.037. PubMed PMID: 32991844;
645 PubMed Central PMCID: PMCPMC7494283.

646 42. Graham C, Seow J, Huettner I, Khan H, Kouphou N, Acors S, et al. Neutralization
647 potency of monoclonal antibodies recognizing dominant and subdominant epitopes on
648 SARS-CoV-2 Spike is impacted by the B.1.1.7 variant. *Immunity*. 2021;54(6):1276-
649 89.e6. Epub 2021/04/10. doi: 10.1016/j.immuni.2021.03.023. PubMed PMID: 33836142;
650 PubMed Central PMCID: PMCPMC8015430.

651 43. Tong P, Gautam A, Windsor IW, Travers M, Chen Y, Garcia N, et al. Memory B cell
652 repertoire for recognition of evolving SARS-CoV-2 spike. *Cell*. 2021;184(19):4969-
653 80.e15. Epub 2021/08/02. doi: 10.1016/j.cell.2021.07.025. PubMed PMID: 34332650;
654 PubMed Central PMCID: PMCPMC8299219.

655 44. Wec AZ, Wrapp D, Herbert AS, Maurer DP, Haslwanter D, Sakharkar M, et al. Broad
656 neutralization of SARS-related viruses by human monoclonal antibodies. *Science*.
657 2020;369(6504):731-6. Epub 2020/06/17. doi: 10.1126/science.abc7424. PubMed PMID:
658 32540900; PubMed Central PMCID: PMCPMC7299279.

659 45. Scheid JF, Barnes CO, Eraslan B, Hudak A, Keeffe JR, Cosimi LA, et al. B cell
660 genomics behind cross-neutralization of SARS-CoV-2 variants and SARS-CoV. *Cell*.
661 2021;184(12):3205-21.e24. Epub 2021/05/21. doi: 10.1016/j.cell.2021.04.032. PubMed
662 PMID: 34015271; PubMed Central PMCID: PMCPMC8064835.

663 46. Hurlburt NK, Seydoux E, Wan YH, Edara VV, Stuart AB, Feng J, et al. Structural basis
664 for potent neutralization of SARS-CoV-2 and role of antibody affinity maturation. *Nat
665 Commun*. 2020;11(1):5413. Epub 2020/10/29. doi: 10.1038/s41467-020-19231-9.
666 PubMed PMID: 33110068; PubMed Central PMCID: PMCPMC7591918.

667 47. Reincke SM, Yuan M, Kornau H-C, Corman VM, van Hoof S, Sánchez-Sendin E, et al.
668 SARS-CoV-2 Beta variant infection elicits potent lineage-specific and cross-reactive
669 antibodies. *bioRxiv*. 2021. doi: 10.1101/2021.09.30.462420.

670 48. Schmitz AJ, Turner JS, Liu Z, Zhou JQ, Aziati ID, Chen RE, et al. A vaccine-induced
671 public antibody protects against SARS-CoV-2 and emerging variants. *Immunity*.
672 2021;54(9):2159-66.e6. Epub 2021/09/01. doi: 10.1016/j.immuni.2021.08.013. PubMed
673 PMID: 34464596; PubMed Central PMCID: PMCPMC8367776.

674 49. Andreano E, Paciello I, Piccini G, Manganaro N, Pileri P, Hyseni I, et al. Hybrid immunity
675 improves B cells and antibodies against SARS-CoV-2 variants. *Nature*. 2021. Epub
676 2021/10/21. doi: 10.1038/s41586-021-04117-7. PubMed PMID: 34670266.

677 50. Li T, Han X, Gu C, Guo H, Zhang H, Wang Y, et al. Potent SARS-CoV-2 neutralizing
678 antibodies with protective efficacy against newly emerged mutational variants. *Nat
679 Commun*. 2021;12(1):6304. Epub 2021/11/04. doi: 10.1038/s41467-021-26539-7.
680 PubMed PMID: 34728625.

681 51. Wheatley AK, Pymm P, Esterbauer R, Dietrich MH, Lee WS, Drew D, et al. Landscape
682 of human antibody recognition of the SARS-CoV-2 receptor binding domain. *Cell Rep*.
683 2021;37(2):109822. Epub 2021/10/06. doi: 10.1016/j.celrep.2021.109822. PubMed
684 PMID: 34610292; PubMed Central PMCID: PMCPMC8463300.

685 52. Benson DA, Cavanaugh M, Clark K, Karsch-Mizrachi I, Lipman DJ, Ostell J, et al.
686 GenBank. *Nucleic Acids Res*. 2013;41(Database issue):D36-42. Epub 2012/11/30. doi:
687 10.1093/nar/gks1195. PubMed PMID: 23193287; PubMed Central PMCID:
688 PMCPMC3531190.

689 53. Flach P, Hernández-Orallo J, Ferri C. A coherent interpretation of AUC as a measure of
690 aggregated classification performance. *Proceedings of the 28th International
691 Conference on International Conference on Machine Learning*; Bellevue, WA, USA2011.
692 p. 657-64.

693 54. Saito T, Rehmsmeier M. The precision-recall plot is more informative than the ROC plot
694 when evaluating binary classifiers on imbalanced datasets. *PLoS One*.
695 2015;10(3):e0118432. Epub 2015/03/05. doi: 10.1371/journal.pone.0118432. PubMed
696 PMID: 25738806; PubMed Central PMCID: PMCPMC4349800.

697 55. Chen EC, Gilchuk P, Zost SJ, Suryadevara N, Winkler ES, Cabel CR, et al. Convergent
698 antibody responses to the SARS-CoV-2 spike protein in convalescent and vaccinated
699 individuals. *Cell Rep*. 2021;36(8):109604. Epub 2021/08/20. doi:
700 10.1016/j.celrep.2021.109604. PubMed PMID: 34411541; PubMed Central PMCID:
701 PMCPMC8352653.

702 56. Lang S, Xie J, Zhu X, Wu NC, Lerner RA, Wilson IA. Antibody 27F3 broadly targets
703 influenza A group 1 and 2 hemagglutinins through a further variation in VH1-69 antibody
704 orientation on the HA stem. *Cell Rep*. 2017;20(12):2935-43. doi:
705 10.1016/j.celrep.2017.08.084. PubMed PMID: 28930686.

706 57. Dreyfus C, Laursen NS, Kwaks T, Zuidgeest D, Khayat R, Ekiert DC, et al. Highly
707 conserved protective epitopes on influenza B viruses. *Science*. 2012;337(6100):1343-8.
708 doi: 10.1126/science.1222908. PubMed PMID: 22878502; PubMed Central PMCID:
709 PMCPMC3538841.

710 58. Sui J, Hwang WC, Perez S, Wei G, Aird D, Chen LM, et al. Structural and functional
711 bases for broad-spectrum neutralization of avian and human influenza A viruses. *Nat
712 Struct Mol Biol*. 2009;16(3):265-73. doi: 10.1038/nsmb.1566. PubMed PMID: 19234466;
713 PubMed Central PMCID: PMCPMC2692245.

714 59. Ekiert DC, Bhabha G, Elsliger MA, Friesen RH, Jongeneelen M, Throsby M, et al.
715 Antibody recognition of a highly conserved influenza virus epitope. *Science*.
716 2009;324(5924):246-51. doi: 10.1126/science.1171491. PubMed PMID: 19251591;
717 PubMed Central PMCID: PMCPMC2758658.

718 60. Wu NC, Andrews SF, Raab JE, O'Connell S, Schramm CA, Ding X, et al. Convergent
719 evolution in breadth of two VH6-1-encoded influenza antibody clonotypes from a single
720 donor. *Cell Host Microbe*. 2020;28:434-44. Epub 2020/07/04. doi:
721 10.1016/j.chom.2020.06.003. PubMed PMID: 32619441.

722 61. Joyce MG, Wheatley AK, Thomas PV, Chuang GY, Soto C, Bailer RT, et al. Vaccine-
723 induced antibodies that neutralize group 1 and group 2 influenza A viruses. *Cell*.
724 2016;166(3):609-23. doi: 10.1016/j.cell.2016.06.043. PubMed PMID: 27453470;
725 PubMed Central PMCID: PMCPMC4978566.

726 62. Kallewaard NL, Corti D, Collins PJ, Neu U, McAuliffe JM, Benjamin E, et al. Structure
727 and function analysis of an antibody recognizing all influenza A subtypes. *Cell*.
728 2016;166(3):596-608. doi: 10.1016/j.cell.2016.05.073. PubMed PMID: 27453466;
729 PubMed Central PMCID: PMCPMC4967455.

730 63. Robbiani DF, Bozzacco L, Keeffe JR, Khouri R, Olsen PC, Gazumyan A, et al. Recurrent
731 potent human neutralizing antibodies to Zika virus in Brazil and Mexico. *Cell*.
732 2017;169(4):597-609.e11. Epub 2017/05/06. doi: 10.1016/j.cell.2017.04.024. PubMed
733 PMID: 28475892; PubMed Central PMCID: PMCPMC5492969.

734 64. Winters A, McFadden K, Bergen J, Landas J, Berry KA, Gonzalez A, et al. Rapid single
735 B cell antibody discovery using nanopores and structured light. *mAbs*. 2019;11(6):1025-
736 35. Epub 2019/06/13. doi: 10.1080/19420862.2019.1624126. PubMed PMID: 31185801;
737 PubMed Central PMCID: PMCPMC6748590.

738 65. Curtis NC, Lee J. Beyond bulk single-chain sequencing: Getting at the whole receptor.
739 *Curr Opin Syst Biol*. 2020;24:93-9. Epub 2020/10/27. doi: 10.1016/j.coisb.2020.10.008.
740 PubMed PMID: 33102951; PubMed Central PMCID: PMCPMC7568503.

741 66. Ye J, Ma N, Madden TL, Ostell JM. IgBLAST: an immunoglobulin variable domain
742 sequence analysis tool. *Nucleic Acids Res*. 2013;41(Web Server issue):W34-40. doi:
743 10.1093/nar/gkt382. PubMed PMID: 23671333; PubMed Central PMCID:
744 PMCPMC3692102.

745 67. Shiakolas AR, Kramer KJ, Wrapp D, Richardson SI, Schafer A, Wall S, et al. Cross-
746 reactive coronavirus antibodies with diverse epitope specificities and Fc effector
747 functions. *Cell Rep Med*. 2021;2(6):100313. Epub 2021/06/01. doi:
748 10.1016/j.xcrm.2021.100313. PubMed PMID: 34056628; PubMed Central PMCID:
749 PMCPMC8139315.

750 68. Tareen A, Kinney JB. Logomaker: beautiful sequence logos in Python. *Bioinformatics*.
751 2020;36(7):2272-4. Epub 2019/12/11. doi: 10.1093/bioinformatics/btz921. PubMed
752 PMID: 31821414; PubMed Central PMCID: PMCPMC7141850.

753 69. Dunbar J, Deane CM. ANARCI: antigen receptor numbering and receptor classification.
754 *Bioinformatics*. 2016;32(2):298-300. Epub 2015/10/02. doi:

755 10.1093/bioinformatics/btv552. PubMed PMID: 26424857; PubMed Central PMCID:
756 PMCPMC4708101.

757 70. Vaswani A, Shazeer N, Parmar N, Uszkoreit J, Jones L, Gomez AN, et al. Attention is all
758 you need. 31st Conference on Neural Information Processing Systems (NIPS 2017);
759 Long Beach, CA, USA2017.

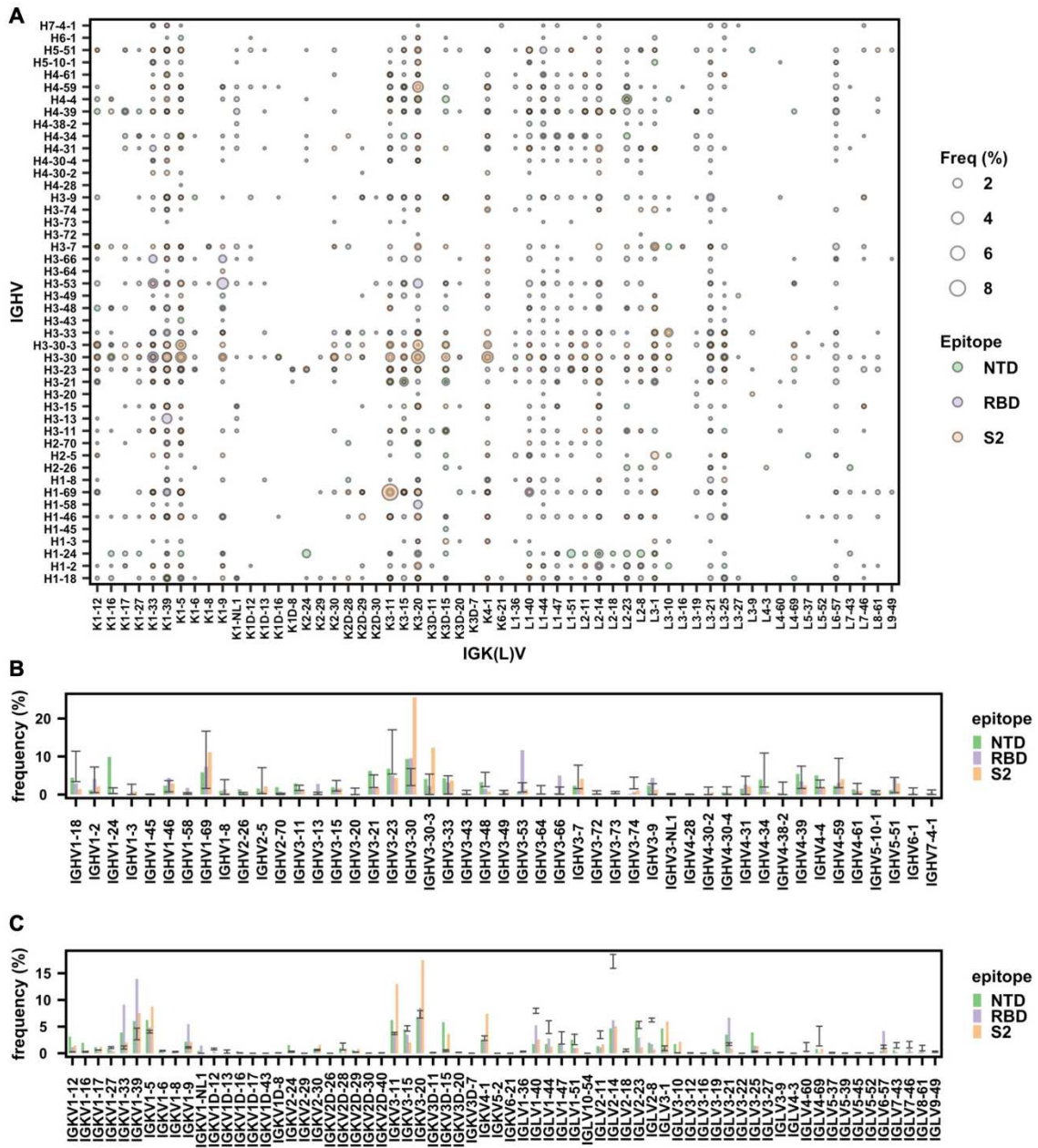
760 71. Srivastava N, Hinton G, Krizhevsky A, Sutskever I, Salakhutdinov R. Dropout: A simple
761 way to prevent neural networks from overfitting. *J Mach Learn Res.* 2014;15:1929-58.

762 72. Soto C, Finn JA, Willis JR, Day SB, Sinkovits RS, Jones T, et al. PyIR: a scalable
763 wrapper for processing billions of immunoglobulin and T cell receptor sequences using
764 IgBLAST. *BMC Bioinformatics.* 2020;21(1):314. Epub 2020/07/18. doi: 10.1186/s12859-
765 020-03649-5. PubMed PMID: 32677886; PubMed Central PMCID: PMCPMC7364545.

766 73. Abadi M, Barham P, Chen J, Chen Z, Davis A, Dean J, et al., editors. *TensorFlow: A*
767 *system for large-scale machine learning.* Proceedings of the 12th USENIX Symposium
768 *on Operating Systems Design and Implementation;* 2016; Savannah, GA, USA.

769 74. Krissinel E, Henrick K. Inference of macromolecular assemblies from crystalline state. *J*
770 *Mol Biol.* 2007;372(3):774-97. Epub 2007/08/08. doi: 10.1016/j.jmb.2007.05.022.
771 PubMed PMID: 17681537.

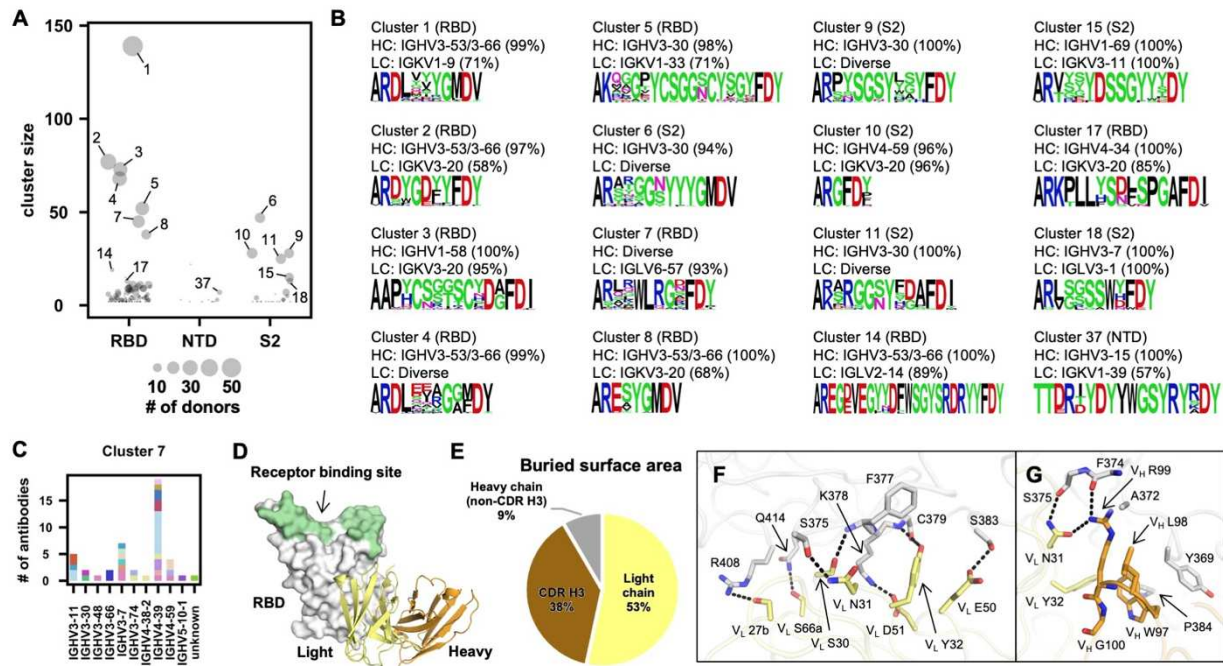
772



773

774 **Figure 1. Analysis of V gene usage in SARS-CoV-2 S antibodies. (A)** The frequency of
775 different V gene pairings between heavy and light chains are shown for SARS-CoV-2 S antibodies
776 to RBD, NTD, and S2. The size of each datapoint represents the frequency of the corresponding
777 IGHV/IGK(L)V pair within its epitope category. Only those antibodies where both IGHV and
778 IGK(L)V information is available for both heavy and light chains was included in this analysis. **(B)**
779 The IGHV gene usage in antibodies to NTD, RBD, and S2 are shown. Only those antibodies with

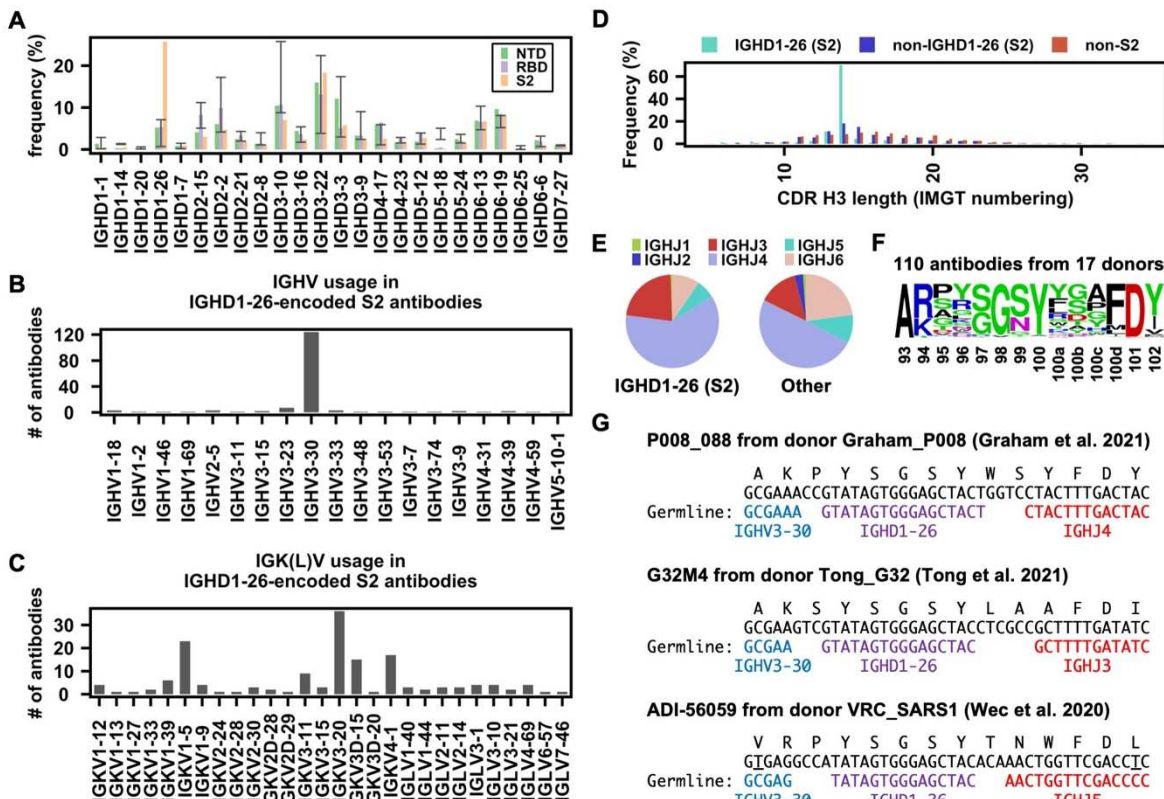
780 IGHV information available were included in this analysis. **(C)** The IGK(L)V gene usage in
781 antibodies to NTD, RBD, and S2 are shown. Only those antibodies with IGK(L)V information
782 available were included in this analysis. **(B-C)** Error bars represent the frequency range among
783 26 healthy donors [31-33].



784

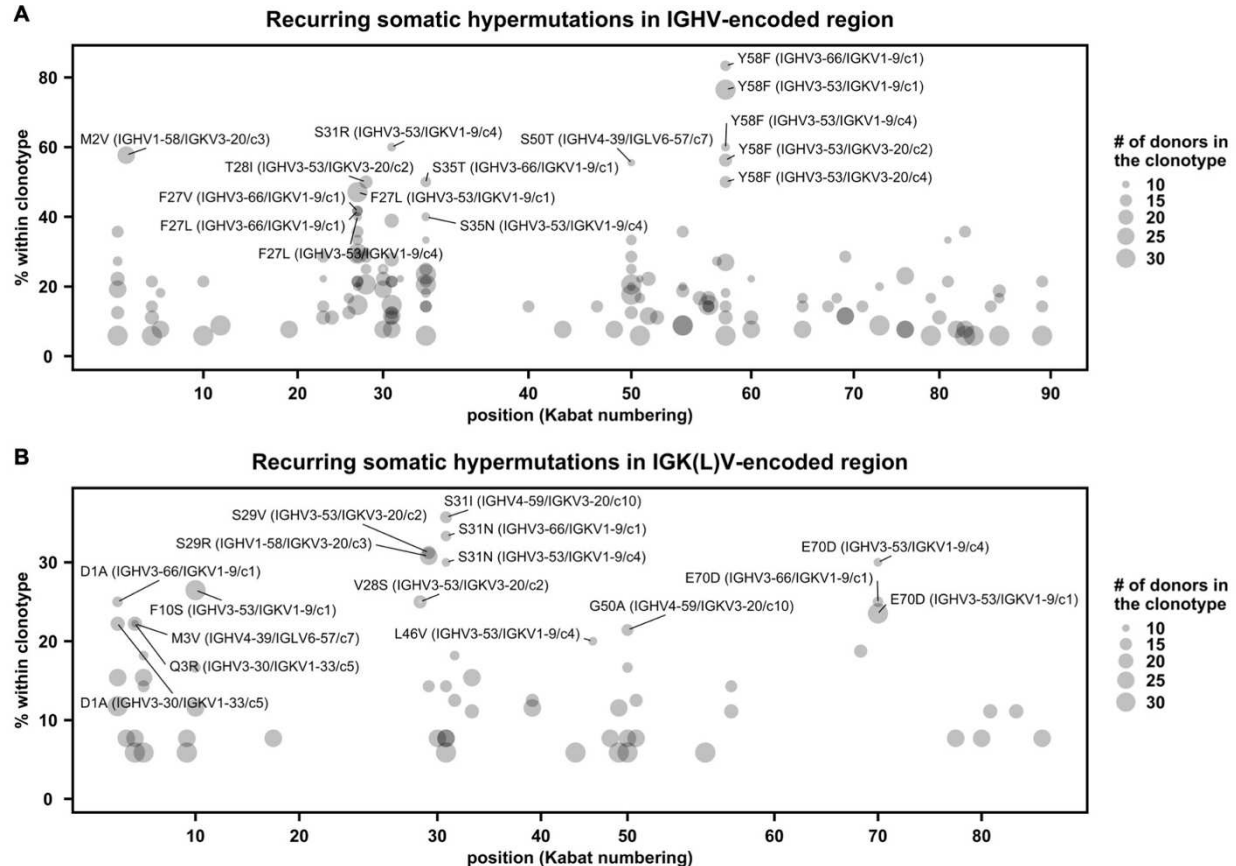
785 **Figure 2. Convergent CDR H3 sequences among SARS-CoV-2 S antibodies. (A)** CDR H3
 786 sequences from individual antibodies were clustered using a 20% cutoff (see Materials and
 787 Methods). The epitope of each CDR H3 cluster is classified based on that of its antibody
 788 members. Cluster size represents the number of antibodies within the cluster. **(B)** The V gene
 789 usage and CDR H3 sequence are shown for each of the 16 CDR H3 clusters of interest. For each
 790 of the CDR H3 cluster of interest, the CDR H3 sequences are shown as a sequence logo, where
 791 the height of each letter represents the frequency of the corresponding amino-acid variant (single-
 792 letter amino-acid code) at the indicated position. The dominant germline V genes (>50% usage
 793 among all antibodies within a given CDR H3 cluster) are listed. Diverse: no germline V genes had
 794 >50% frequency among all antibodies within a given CDR H3 cluster. HC: heavy chain. LC: light
 795 chain. **(C)** IGHV usage in cluster 7 is shown. Different colors represent different donors. Unknown:
 796 IGHV information is not available. **(D)** An overall view of SARS-CoV-2 RBD in complex with
 797 IGLV6-57 antibody S2A4 (PDB 7JVA) [41], which belongs to cluster 7, is shown. The RBD is in
 798 white with the receptor binding site highlighted in green. The heavy and light chains of S2A4 are
 799 in orange and yellow, respectively. **(E)** Percentages of the S2A4 epitope that are buried by the

800 light chain, heavy chain (without CDR H3), and CDR H3 are shown as a pie chart. Buried surface
801 area (BSA) was calculated by PISA (Proteins, Interfaces, Structures and Assemblies) at the
802 European Bioinformatics Institute (https://www.ebi.ac.uk/pdbe/prot_int/pistart.html) [74]. **(F-G)**
803 Detailed interactions between the **(F)** light and **(G)** heavy chains of S2A4 and SARS-CoV-2 RBD.
804 Hydrogen bonds and salt bridges are represented by black dashed lines. The color coding is the
805 same as panel D.



806

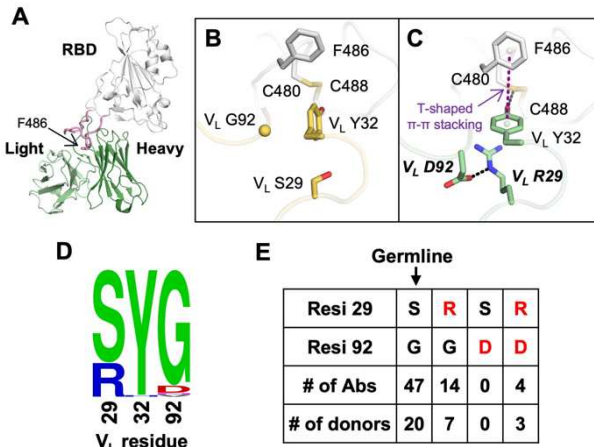
807 **Figure 3. Enrichment of IGHD1-26 in SARS-CoV-2 S2 antibodies. (A)** The IGHD gene usage
 808 in NTD, RBD, S2 antibodies is shown. Error bars represent the frequency range among 26 healthy
 809 donors. **(B)** IGHV gene usage and **(C)** IGK(L)V gene usage among IGHD1-26 S2 antibodies is
 810 shown (n = 157). **(D)** The distribution of CDR H3 length (IMGT numbering) in IGHD1-26 S2
 811 antibodies (n = 157), non-IGHD1-26 S2 antibodies (n = 533), and other non-S2 S antibodies that
 812 do not target S2 (n = 5,090), are shown. **(E)** The IGHJ gene usage among IGHD1-26 S2
 813 antibodies (n = 157) and other S antibodies with well-defined epitopes (n = 5,623) is shown. **(F)**
 814 The CDR H3 sequences for IGHD1-26 S2 antibodies (n = 110) are shown as a sequence logo.
 815 **(G)** Amino acid and nucleotide sequences of the V-D-J junction are shown for three IGHD1-26
 816 S2 antibodies [42-44]. Putative germline sequences and segments were identified by IgBlast [66]
 817 and are indicated. Somatically mutated nucleotides are underlined. Intervening spaces at the V-
 818 D and D-J junctions are N-nucleotide additions.



819

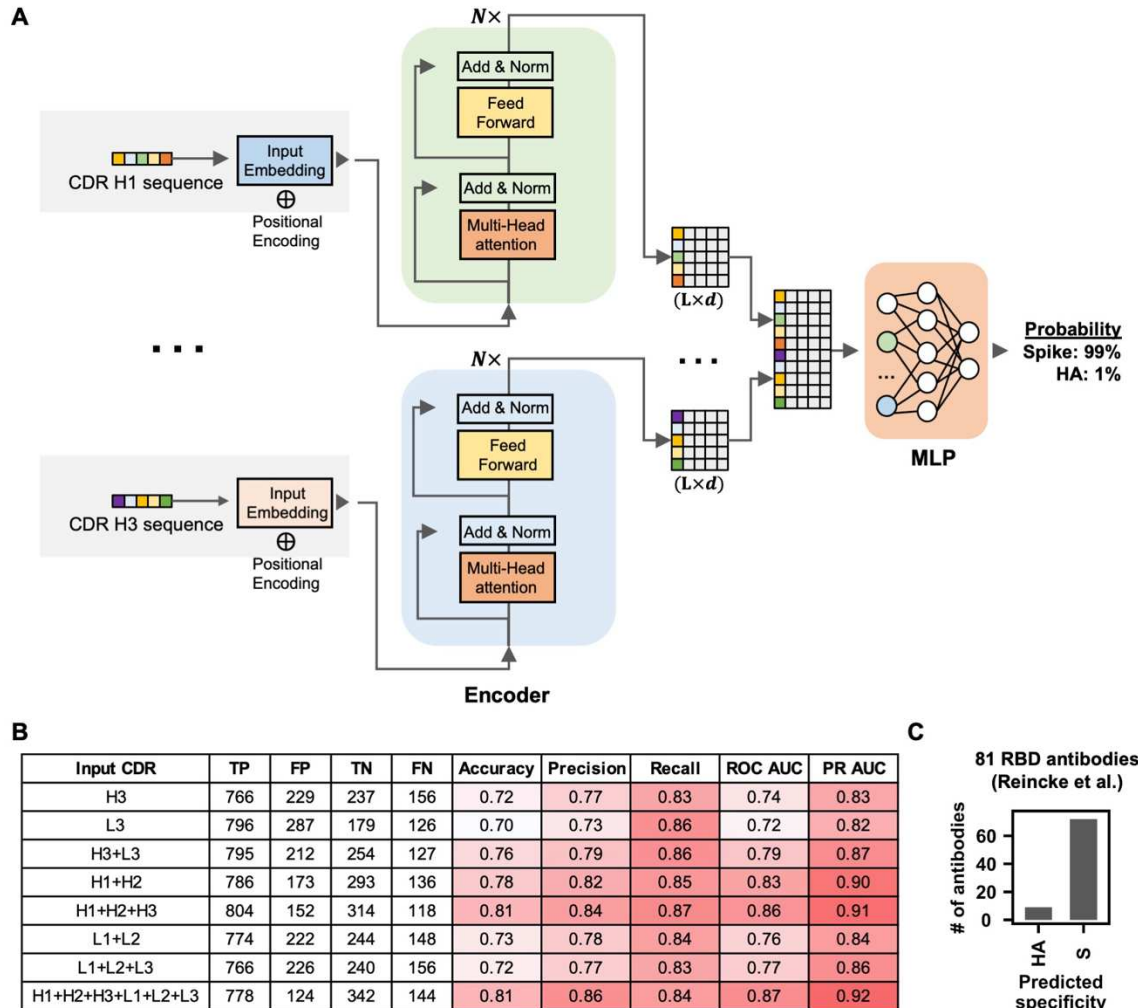
820 **Figure 4. Recurring somatic hypermutations (SHMs) in SARS-CoV-2 S antibodies. (A-B)** For
 821 each public clonotype, if the exact same SHM emerged in at least two donors, such SHM is
 822 classified as a recurring SHM. Only those public clonotypes that can be observed in at least nine
 823 donors are shown. **(A)** Recurring SHMs in heavy chain V genes. **(B)** Recurring SHMs in light
 824 chain V genes. X-axis represents the position on the V gene (Kabat numbering). Y-axis represents
 825 the percentage of donors who carry a given recurring SHM among those who carry the public
 826 clonotype of interest. For example, V_L S29R emerged in 8 donors out of 26 donors that carry an
 827 public clonotype that is encoded by IGHV1-58/IGKV3-20. As a result, V_L S29R (IGHV1-58/IGKV3-
 828 20) is 31% (8/26) within the corresponding clonotype. Of note, since each public clonotype is also
 829 defined by the similarity of CDR H3 (see Materials and Methods), there could be multiple
 830 clonotypes with the same heavy and light chain V genes (e.g. IGHV3-53/IGKV1-9). The CDR H3
 831 cluster ID for each clonotype is indicated with a prefix “c”, following the information of the V genes.

832 For heavy chain, SHMs that emerged in at least 40% of the donors of the corresponding clonotype
833 are labeled. For light chain, SHMs that emerged in at least 20% of the donors of the corresponding
834 clonotype are labeled.



835

836 **Figure 5. Structural analysis of a recurring SHM in the IGHV1-58/IGKV3-20 public**
837 **clonotype. (A)** An overall view of SARS-CoV-2 RBD in complex with the IGHV1-58/IGKV3-20
838 antibody PDI 222 (PDB 7RR0) [51]. The RBD is shown in white, while the heavy and light chains
839 of the antibody are in dark and light green, respectively. The ridge region (residues 471-491) is
840 shown in pink, with F486 highlighted as sticks. **(B-C)** Structural comparison between two IGHV1-
841 58/IGKV3-20 antibodies that either **(B)** carry germline residues V_L S29/G92 (COVOX-253, PDB
842 7BEN) [40] and **(C)** somatically hypermutated residues V_L R29/D92 (PDI 222, PDB 7RR0) [51].
843 SARS-CoV-2 RBD is in white, while antibodies are in yellow (COVOX-253) and green (PDI 222).
844 Somatically mutated residues are labeled with bold and italic letters. The T-shaped π - π stacking
845 between RBD-F486 and V_L Y32 is indicated by a purple dashed line. Hydrogen bond and salt
846 bridge are represented by black dashed lines. **(D)** Sequence logo of V_L residues 29, 32, and 92
847 among 67 IGHV1-58/IGKV3-20 RBD antibodies are shown. **(E)** Numbers of antibodies in the
848 IGHV1-58/IGKV3-20 public clonotype carrying the germline-encoded variant at V_L residues 29
849 and 92 (S29, G92), as well as V_L SHM S29R and G92D (red) are listed. Of note, one antibody in
850 this IGHV1-58/IGKV3-20 public clonotype carries S29/N92 and another carries S29/V92.
851 However, they are not listed in the table here.



852

853 **Figure 6. Antigen identification by deep learning. (A)** A schematic overview of the deep
 854 learning model architecture. **(B)** For evaluating model performance, S antibodies and HA
 855 antibodies were considered “positive” and “negative”, respectively. Model performance on the
 856 test set was compared when different input types were used. Of note, the test set has no
 857 overlap with the training set and the validation set, both of which were used to construct the
 858 deep learning model. True positive (TP) represents the number of S antibodies being correctly
 859 classified as S antibodies. False positive (FP) represents the number of HA antibodies being
 860 misclassified as S antibodies. True negative (TN) represents the number of HA antibodies being
 861 correctly classified as HA antibodies. False negative (FN) represents the number of S

862 antibodies being misclassified as HA antibodies. See Materials and Methods for the calculations
863 of accuracy, precision, recall, ROC AUC, and PR AUC for the training and test sets. **(C)** The
864 antigen specificity of 81 RBD antibodies from Reincke et al. [47] were predicted by a deep
865 learning model that was trained to distinguish between S antibodies and HA antibodies.